Peptide-guided resiquimod-loaded lignin nanoparticles convert tumor-associated macrophages from M2 to M1 phenotype for enhanced chemotherapy

Figueiredo, Patricia

2021-10-01

Figueiredo , P , Lepland , A , Scodeller , P , Fontana , F , Torrieri , G , Tiboni , M , Shahbazi , M-A , Casettari , L , Kostiainen , M , Hirvonen , J , Teesalu , T & Santos , H A 2021 , ' Peptide-guided resiquimod-loaded lignin nanoparticles convert tumor-associated macrophages from M2 to M1 phenotype for enhanced chemotherapy ' , Acta Biomaterialia , vol. 133 , pp. 231-243 . https://doi.org/10.1016/j.actbio.2020.09.038

http://hdl.handle.net/10138/348345
https://doi.org/10.1016/j.actbio.2020.09.038

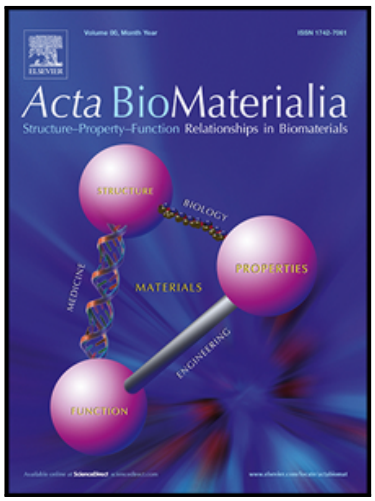

Peptide-guided resiquimod-loaded lignin nanoparticles convert tumor-associated macrophages from M2 to M1 phenotype for enhanced chemotherapy

Patrícia Figueiredo , Anni Lepland , Pablo Scodeller , Flavia Fontana , Giulia Torrieri , Mattia Tiboni , Mohammad-Ali Shahbazi , Luca Casettari , Mauri A. Kostiainen , Jouni Hirvonen , Tambet Teesalu , Hélder A. Santos

PII: S1742-7061(20)30561-4
DOI: https://doi.org/10.1016/j.actbio.2020.09.038
Reference: ACTBIO 6953

To appear in: *Acta Biomaterialia*

Received date: 10 August 2020
Revised date: 23 September 2020
Accepted date: 24 September 2020

Please cite this article as: Patrícia Figueiredo , Anni Lepland , Pablo Scodeller , Flavia Fontana , Giulia Torrieri , Mattia Tiboni , Mohammad-Ali Shahbazi , Luca Casettari , Mauri A. Kostiainen , Jouni Hirvonen , Tambet Teesalu , Hélder A. Santos , Peptide-guided resiquimod-loaded lignin nanoparticles convert tumor-associated macrophages from M2 to M1 phenotype for enhanced chemotherapy, *Acta Biomaterialia* (2020), doi: https://doi.org/10.1016/j.actbio.2020.09.038

Peptide-guided resiquimod-loaded lignin nanoparticles convert tumor-associated macrophages from M2 to M1 phenotype for enhanced chemotherapy

Patrícia Figueiredo[a,*] patricia.figueiredo@helsinki.fi, Anni Lepland[b], Pablo Scodeller[b,*] pablo.david.scodeller@ut.ee, Flavia Fontana[a], Giulia Torrieri[a], Mattia Tiboni[c], Mohammad-Ali Shahbazi[a,d], Luca Casettari[c], Mauri A. Kostiainen[e], Jouni Hirvonen[a], Tambet Teesalu[b,f,g,*] tambet.teesalu@ut.ee, and Hélder A. Santos[a,h,*] helder.santos@helsinki.fi

[a]Drug Research Program, Division of Pharmaceutical Chemistry and Technology, Faculty of Pharmacy, University of Helsinki, FI-00014 Helsinki, Finland

[b]Laboratory of Cancer Biology, Institute of Biomedicine and Translational Medicine, University of Tartu, 50411 Tartu, Estonia

[c]Department of Biomolecular Sciences, School of Pharmacy, University of Urbino Carlo Bo, Urbino, Italy

[d]Department of Pharmaceutical Nanotechnology, School of Pharmacy, Zanjan University of Medical Sciences, 56184-45139 Zanjan, Iran

[e]Biohybrid Materials, Department of Bioproducts and Biosystems, Aalto University, FI-00076, Aalto, Finland

[f]Center for Nanomedicine and Department of Cell, Molecular and Developmental Biology, University of California, Santa Barbara, 93106, CA, USA

[g]Cancer Research Center, Sanford Burnham Prebys Medical Discovery Institute, La Jolla, 92037, CA, USA

[h]Helsinki Institute of Life Science (HiLIFE), University of Helsinki, FI-00014 Helsinki, Finland

[*]Corresponding authors.

Highlights

- Functionalization of resiquimod-loaded lignin nanoparticles with the “mUNO” peptide to target the CD206-positive M2-like TAMs.
- Shifting the immune cells in the tumor microenvironment towards an anti-tumor immune state, by increasing the representation of M1-like macrophages, cytotoxic T cells, and activated dendritic cells.
- Enhances the anticancer effect of the vinblastine when co-administered with resiquimod-loaded LNPs decorated with mUNO.

Abstract

Nanomedicines represent innovative and promising alternative technologies to improve the therapeutic effects of different drugs for cancer ablation. Targeting M2-like tumor-associated macrophages (TAMs) has emerged as a favorable therapeutic approach to fight against cancer through the modulation of the tumor microenvironment. However, the immunomodulatory molecules used for this purpose present side effects upon systemic administration, which limits their

clinical translation. Here, the biocompatible lignin polymer is used to prepare lignin nanoparticles (LNPs) that carry a dual agonist of the toll-like receptors TLR7/8 (resiquimod, R848). These LNPs are targeted to the CD206-positive M2-like TAMs using the "mUNO" peptide, in order to revert their pro-tumor phenotype into anti-tumor M1-like macrophages in the tumor microenvironment of an aggressive triple-negative in vivo model of breast cancer. Overall, we show that targeting the resiquimod (R848)-loaded LNPs to the M2-like macrophages, using very low doses of R848, induces a profound shift in the immune cells in the tumor microenvironment towards an anti-tumor immune state, by increasing the representation of M1-like macrophages, cytotoxic T cells, and activated dendritic cells. This effect consequently enhances the anticancer effect of the vinblastine (Vin) when co-administered with R848-loaded LNPs.

Keywords

lignin nanoparticles; resiquimod; macrophage repolarization; mannose receptor; mUNO

1. Introduction

Several nanoplatforms have been employed for cancer immunotherapy, where biomaterials with immunostimulatory properties can be used to formulate cancer vaccines, or other nanomaterials can load and deliver different immunomodulatory compounds [1–5]. Additionally, cancer nanomedicines represent a promising alternative over the conventional therapies to overcome their limitations, including the poor water solubility, the lack of anti-tumor specificity, and consequent systemic side effects [6–8]. For this purpose, different types of nanomaterials have been developed, such as inorganic nanoparticles (NPs) [9,10], lipid-based nanosystems [11–13], and polymeric NPs [14–18]. Lignocellulosic materials, such as cellulose, hemicellulose, and lignin, have gained increased attention, as they are derived from natural sources, are largely abundant in nature, and are biocompatible and biodegradable [19,20]. In particular, lignin has been recently used as a drug delivery vehicle, after transforming the raw material into lignin NPs (LNPs), using different approaches like antisolvent precipitation, solvent exchange or sonication [19,21–23]. Additionally, the functional groups on the original lignin polymer can be chemically modified before preparing the LNPs in order to be functionalized with different targeting moieties, and thus, increase their potential application [19,24,25].

Triple-negative breast cancer (TNBC) is characterized by the lack of molecular targets/receptors, such as estrogen, progesterone, or human epidermal growth factor receptor 2 (HER2), which comprise important molecular targets for different therapeutic agents, and therefore, it is associated to a poor prognosis compared to other breast cancer subtypes [26,27]. Additionally, tumor-associated macrophages (TAMs) resembling a pro-tumor M2-like phenotype comprise up to 50% of the tumor mass in breast cancer [28], being usually associated with a worse prognosis, tumor progression and recurrence, higher risk of distant metastasis, and suppression of other effector cells like $CD8^+$ T cells [28–30]. In the tumor microenvironment (TME), TAMs exhibit either an immunosuppressive M2-like phenotype, characterized by the expression of distinctive cell surface markers, including CD163, CD204, and mannose receptor (CD206/MRC1), and increased production of anti-inflammatory signals (*e.g.*, IL-10 and transforming growth factor (TGF)-β, or arginase 1 (ARG 1)), or an anti-tumor M1-like phenotype, in which macrophages can express MHC-II, CD68, CD86, and CD80 cell surface markers, release pro-inflammatory cytokines (*e.g.*, interleukin (IL)-12, IL-1β, IL-6 and tumor necrosis factor (TNF)-α), and produce reactive oxygen species (ROS) [31–34]. Targeting therapeutics to TME components like TAMs can be seen as a complementary approach to chemotherapy, the primary established systemic treatment choice for patients with both early-stage and advanced-stage TNBC, to improve the therapeutic outcome [35]. Emerging therapies that aim to target TAMs comprise the inhibition of monocyte/macrophage recruitment to the tumor tissue, after blocking colony-stimulating factor 1 (CSF-1) receptor or CCL2-CCR2 signaling pathway [36–38], elimination or depletion of TAMs in the TME, by triggering their apoptosis and delay the tumor progression [34,39], and reversion or reprogramming the immunosuppressive M2-like phenotype towards a tumoricidal M1-like TAMs, by manipulating the environmental stimuli [34,39–43]. However, these approaches are usually associated with a lack of specific targeting and consequent systemic side effects, which limit their

application in the clinic [34,39]. In order to circumvent these limitations, nanomedicines can be tailored to carry therapeutics and effectively target them to the TAMs at the tumor site [44,45].

In this study, we took advantage of the lignin biopolymer as starting material to prepare LNPs, and employ them as a drug delivery vehicle to carry resiquimod (R848), a dual agonist of the toll-like receptors TLR7/8 that can promote the repolarization of M2-like into M1-like TAMs, yielding R848@LNPs [46]. The R848@LNPs were further functionalized with 5(6)-carboxyfluorescein (FAM)-labeled hexapeptide (sequence: CSPGAK, "mUNO") that targets the mannose receptor (CD206), typically overexpressed in the M2-like macrophages (Asciutto et al., 2019; Lepland et al., 2020; Scodeller et al., 2017). The *in vitro* cytocompatibility of both non-targeted and targeted R848@LNPs, hereafter referred to as R848@LNPs-P-FAM and R848@LNPs-P-F-mUNO, respectively, was evaluated towards mouse derived M2-like macrophages, and their repolarization effect was assessed by evaluating the expression levels of the cell surface markers CD86 and CD206, and the production of ROS, such as hydrogen peroxide (H_2O_2), and also TNF-α. *In vivo* biodistribution studies were conducted to analyze the homing ability of R848@LNPs towards the M2-like TAMs in orthotopic 4T1 tumor-bearing mice, an aggressive TNBC preclinical model. Finally, a chemotherapeutic compound (Vinblastine, Vin) was co-administered with free R848 or R848@LNPs for synergetic anticancer effect in the same TNBC model, and the immunological profile of the cell population in the tumor tissues was evaluated.

2. Materials and Methods

2.1. Materials

BioPiva™ softwood kraft lignin was acquired from UPM Biochemicals (Finland). Maleimide-poly(ethylene glycol)-amine (Mal-PEG-NH_2, 2K) was obtained from Biochempeg Scientific Inc. (Watertown, MA, USA). 5(6)-carboxyfluorescein (FAM)-Ahx-Cys-NH_2 and FAM-Ahx-CSPGAK-COOH (mUNO) (hereafter referred to as FAM and FAM-mUNO, respectively) were purchased from TAG Copenhagen (Denmark). Resiquimod (R848) was purchased from DC Chemicals (Shanghai, China). 4-(2-hydroxyethyl)-1-piperazineethanesulfonic acid (HEPES), tetrahydrofuran (THF), *N*-hydroxysuccinimide (NHS), 1-ethyl-3-(3-dimethylaminopropyl)carbodiimide (EDC) and 2-(*N*-morpholino)ethanesulfonic acid (MES) were obtained from Sigma-Aldrich®, USA. Culture flasks were acquired from Corning Inc., USA. Roswell Park Memorial Institute 1640 medium (RPMI), fetal bovine serum (FBS), non-essential amino acids (NEAA), L-glutamine (200 mM), streptomycin (100 mg/mL), penicillin (100 IU/mL) and trypsin (2.5%) were purchased from HyClone Waltham, USA. Hank's balanced salt solution (10 × HBSS) and Dulbecco's phosphate buffer saline (10 × PBS) were obtained from Life Technologies Gibco® (Carlsbad, CA, USA).

2.2. Preparation and characterization of LNPs

Carboxylated lignin was prepared in order to increase the number of carboxyl groups on the lignin structure for further conjugation reactions, using a ratio of original lignin:succinic anhydride of 4:1, as previously described and characterized [25].

The LNPs were prepared by solvent exchange and formed during the dialysis process against MilliQ-water that took place during 24 h, after introducing 1 mg/mL of carboxylated lignin in THF into a dialysis bag (Spectra/Por® 1 Standard RC Dry Dialysis Tubing, 12-14 kDa, Spectrum Labs, USA), as done previously [25,50]. For drug loading, the R848 was dissolved in EtOH and mixed with the lignin solution in THF, using a mass ratio R848:lignin of 1:10, introduced into a dialysis membrane, and the R848-loaded LNPs (R848@LNPs) were formed during the solvent exchange process against MilliQ-water for 24 h in order to get rid of the THF and free R848.

The prepared LNPs and R848@LNPs were characterized for their average particle size (Z-average), polydispersity index (PDI), and average zeta (ζ)-potential (surface charge) by dynamic light scattering (DLS), using a Malvern Zetasizer Nano ZS instrument (Malvern Instruments Ltd, UK). After placing the LNP droplet on a carbon-coated copper grid, and let the grid to dry before analysis, both LNPs and R848@LNPs were morphologically characterized, using a transmission electron microscopy (TEM, Jeol JEM-1400, Jeol Ltd., Tokyo, Japan), with an acceleration voltage of 80 kV. The LNPs were also characterized with FTIR

instrument (Vertex 70, Bruker, USA) using a horizontal ATR accessory (MIRacle, PIKE Technologies, USA). The ATR–FTIR spectra were recorded at room temperature between 4000–650 cm^{-1} with a resolution of 4 cm^{-1} using OPUS 5.5 software.

2.3. Functionalization of LNPs with FAM and FAM-mUNO

The mass ratios for the conjugation reactions were chosen after optimization of the conjugation parameters. The reaction between the –COOH groups of LNPs and $–NH_2$ groups of Mal-PEG-NH_2 was done using EDC/NHS coupling chemistry. For that, 3 mg of LNPs was dispersed in 1.2 mL of 10 mM MES buffer (pH 5.5), with 4.5 µL of EDC (12.8 mM) and 1.2 mg of NHS (8.7 mM), and the mixture was reacted under stirring for 1 h, in the dark and at room temperature (RT), to activate the carboxyl groups on the LNPs. After spinning down the mixture to remove excess EDC/NHS (16100*g* for 5 min), the LNPs were resuspended with 1.5 mL of 10 mM MES buffer (pH 7) containing 15 mg of Mal-PEG-NH_2 (mass ratio 1:5 of LNPs:PEG). The mixture was reacted for 3 h at RT, and subsequently, centrifuged and washed with MilliQ-water to purify the resulting LNPs-PEG-Mal from the free Mal-PEG-NH_2.

Then, the reaction between the cysteine groups of FAM-Cys-NH_2 (FAM) dye and FAM-mUNO (F-mUNO) with the maleimide group on LNPs-PEG-Mal was done in MilliQ-water, resulting in the formation of LNPs-P-FAM and LNPs-P-F-mUNO, respectively. Here, 0.1 mg of FAM/peptide were mixed with 1 mg of LNPs-PEG-Mal, under stirring for 2 h, at RT in the dark. Finally, the prepared LNPs were extensively washed with MilliQ-water to remove unreacted products.

The same protocol described for the empty LNPs was followed for the conjugation reactions with R848@LNPs, in order to obtain R848@LNPs-P-FAM and R848@LNPs-P-F-mUNO. The loading degree (LD) of R848 into LNPs was estimated after dissolving the drug-loaded LNPs with EtOH, and tip-sonicating the LNPs in order to degrade them. After centrifugation at 16100*g* for 5 min, the supernatant was collected to determine the R848 concentration by using high-performance liquid chromatography (HPLC; Agilent 1100 series, Agilent Technologies, USA). The experimental conditions used for quantification of the loaded R848 are described in detail in **Table 1**.

2.4. Stability of R848@LNPs

The stability of R848@LNPs was evaluated by following the changes on their size and PDI, after incubation of 300 µg/mL of bare and functionalized R848@LNPs with RPMI, supplemented with 10% of FBS, at 37°C during 2 h. Samples were withdrawn at 5, 15, 30, 60, 90 and 120 min, and diluted in water for measuring the size and PDI of R848@LNPs. All the experiments were performed in triplicates.

2.5. *In vitro* dissolution study

The *in vitro* release profiles of free R848 and R848-loaded LNPs was performed in two different buffers: 1 × HBSS–MES pH 5.5 (HBSS–MES, pH 5.5) and 1 × HBSS–HEPES pH 7.4 (HBSS–HEPES, pH 7.4). For that, 3 µg of pure R848 and 300 µg of R848@LNPs were immersed in 3 mL of release media, and the samples were stirred at 150 rpm and 37°C. At the scheduled time intervals (5, 10, 15, 30, 60, 120, 240, 360 min and 24 h), 100 µL of the release media were withdrawn, and the same volume of fresh pre-heated release media was added to keep the releasing volume constant. The samples were centrifuged at 16100*g* for 3 min, and the supernatant was collected and analyzed in HPLC. The amount of R848 dissolved over time was determined by measuring the R848 concentration, using the HPLC method described in **Table 1**. The average calculated values were obtained from at least three replicates.

2.6. Cell culturing, isolation of murine BMDMs, and differentiation into macrophages

Murine mammary carcinoma cell line (4T1) was obtained from American Type Culture Collection (ATCC), USA, and further grown in RPMI, supplemented with 10% of FBS, 1% of L-glutamine, and 1% of penicillin-streptomycin (PEST) in 75 cm^2 flasks. Cells were maintained in an incubator (BB 16 gas incubator, Heraeus Instruments GmbH) at 37 °C, 5% CO_2 and 95% relative humidity.

For the isolation of murine bone marrow-derived macrophages (BMDMs), both femur and tibia bones were isolated from female 6-8 week old BALB/c mice, and further cut and flushed with cold PBS (pH 7.4), aided by a 21G needle, to a Petri dish. After, the cell suspension was centrifuged at 500*g* for 5 min, resuspended with 1 mL of Ammonium-Chloride-Potassium (ACK) lysing buffer for 2 min to remove the red blood cells, and then diluted with 9 mL of PBS (pH 7.4) before centrifugation (500*g* for 5 min). The BMDMs were suspended with RPMI (supplemented with 10% of FBS, 1% of PEST and 1% of L-glutamine) and plated in Petri dishes at concentration of 3×10^5 cells per mL, in 10 mL of RPMI containing 20 ng/mL of macrophage colony-stimulating factor (M-CSF, PeproTech, UK), at 37°C. After 3 days, 5 mL of cell culturing medium were replaced by 5 mL fresh RPMI containing 20 ng/mL of M-CSF.[51] After 6 days, resting macrophages (M0 macrophages) were collected and seeded in non-tissue culture treated 48-well plates (Corning Inc., USA) at a density of 2.5×10^5 cells per well, in 0.5 mL of RPMI supplemented with 20 ng/mL of interleukin (IL)-4 (PeproTech, UK) to differentiate into M2-like macrophages, or containing 100 ng/mL of lipopolysaccharide (LPS, Sigma-Aldrich®, USA) and 10 ng/mL of interferon gamma (IFN-γ, PeproTech, UK) in order to obtain M1-like macrophages, and incubated at 37°C for 48 h before characterization.

2.7. Expression of cell surface markers on macrophages

M0, M1, and M2–like macrophages were characterized after incubation with TruStain FcX™ anti-mouse CD16/32 antibody (BioLegend, USA) in cold PBS for 10 min at 4°C, to prevent unspecific interactions. After, anti-mouse Allophycocyanin (APC)–F4/80, Phycoerythrin-Cy7 (PE–Cy7)–CD11b, Alexa Fluor 488–CD86 and APC–CD206 (all from BioLegend, USA) in cold PBS were added to the samples, for 20 min at 4 °C in the dark. After washings, the samples were analyzed by flow cytometry, using a LSR II flow cytometer (BD Biosciences, USA) and FACS Diva software. The data were analyzed by FlowJo V10 software (Tree Star, Ashland, OR, USA) after collecting at least 20000 events. The experiments were performed at least in triplicate.

2.8. Cytocompatibility studies

Both 4T1 cells and M2-like macrophages were seeded in 96-well plates (PerkinElmer Inc., USA) at a density of 1.5×10^4 and 3×10^4 cells per well, respectively, and allowed to attach overnight. Then, 100 µL of empty and R848-loaded LNP suspensions, before and after surface functionalization, were added to each well in cell culturing medium at different concentrations (25–200 µg/mL), and the plates were incubated for 24 h at 37°C. Additionally, similar dilutions for the free R848 (0.8–6.4 µM), previously dissolved with 1% (v/v) EtOH, were added to the cells. Incubations with 1% (v/v) Triton X-100 and cell medium were used as negative and positive controls, respectively. Then, after equilibrating the plates for 30 min at RT, the wells were washed once with 100 µL of HBSS–4-(2-hydroxyethyl)-1-piperazineethanesulfonic acid) (HEPES) buffer. Afterwards, 50 µL of HBSS–HEPES (pH 7.4) was mixed with 50 µL of CellTiter-Glo® (Promega Corporation, USA) in each well, and the plates were stirred on an orbital shaker, protected from the light. Lastly, the luminescence was measured using a Varioskan Flash plate reader (Thermo Fisher Scientific, Inc., NY, USA). The amount of ATP produced by metabolically active cells was used to determine the number of viable cells in culture. The experiments were performed at least in triplicate.

2.9. Immunostainings and *in vitro* cell-LNP association studies

The *in vitro* assessment of the M2-like macrophages-LNP interactions were qualitatively and quantitatively evaluated by confocal microscopy and flow cytometry, respectively.

For flow cytometry, M0 macrophages were seeded in 48-well plates (non-treated cell culture, Corning Inc., USA) at a density of 2.5×10^5 cells per well, in 500 µL of RPMI supplemented with 20 ng/mL of IL-4 to obtain M2-like macrophages, or 100 ng/mL of LPS and 10 ng/mL of IFN-γ in order to obtain M1-like macrophages, for 48 h at 37°C. For the competition study, M2-like

macrophages were previously treated with 200 µL anti-mouse CD206 antibody (10 µg/mL), for 2 h at 37°C, in order to block the CD206 receptor. After washing the cells, 300 µL of empty or R848-loaded LNPs-P-FAM and LNPs-P-F-mUNO (200 µg/mL) were added to each well and incubated at 37°C for 10, 30 or 60 min in complete medium. Then, the wells were washed once with PBS (pH 7.4), and the macrophages were detached using 300 µL of PBS–ethylenediamine tetraacetic acid (EDTA, 5 mM), during 15 min on ice. The cells were collected, centrifuged at 500*g* for 5 min, and suspended in 300 µL PBS–EDTA for flow cytometry analysis, using a LSR II flow cytometer (BD Biosciences, USA) and FACS Diva software. The data were analyzed by FlowJo V10 software (Tree Star, Ashland, OR, USA) after collecting at least 20000 events. All the experiments were performed at least in triplicate.

For confocal microscopy, the 200 µL of M0 macrophages were seeded in Lab-Tek 8- chamber slides (Thermo Fisher Scientific, USA), at a density of 7.5×10^4 cells per well in RPMI supplemented with 20 ng/mL of IL-4, during 48 h, at 37°C. Next, 200 µL of LNPs-P-FAM and LNPs-P-F-mUNO (200 µg/mL) in complete cell culture medium were incubated with the M2-like macrophages for 10, 30 and 60 min, at 37°C. After LNP incubation, the wells were washed once with PBS (pH 7.4), and the cells were fixed with 4% of paraformaldehyde (PFA) for 10 min, at RT. The cells were further permeabilized with 100 µL of 0.2% (v/v) Triton-X in PBS (10 min, RT), and incubated with 100 µL of 5% blocking buffer [5% Bovine serum albumin (BSA) + 5% FBS + 5% Donkey serum in PBS + 0.05% (v/v) Tween-20 (PBS-T)], for 1 h at RT, to prevent unspecific binding of the antibodies. Then, 100 µL of rat anti-mouse CD206 (dilution 1:150) and rabbit anti-FAM (dilution 1:500) in 1% blocking buffer (1% BSA + 1% FBS + 1% Donkey serum in PBS-T) were added to the cells during 1h at RT, followed by the incubation with 100 µL of goat anti-rat Alexa Fluor 647 (dilution 1:250) and goat anti-rabbit Alexa Fluor 488 (dilution 1:500) in 1% of blocking buffer (1% BSA + 1% FBS + 1% Donkey serum in PBS-T), during 35 min at RT. Finally, the nuclei were stained with 200 µL of DAPI (2.8 µg/mL; Thermo Scientific, USA), for 5 min at RT. The wells were washed twice with PBS (pH 7.4) between each staining step. The samples were observed with a Leica SP5 inverted confocal microscope (Leica Microsystems, Germany), using a 63 × /1.2–0.6 oil immersion objective. The colocalization of the LNP FAM signal with $CD206^+$ M2-like macrophages (Pearson's coefficient) was quantified using ImageJ, and the average values were obtained from at least 4 different images.

2.10. Detection of reactive oxygen species

In order to measure the generation of H_2O_2, the non-fluorescent compound 2',7'-dichlorodihydrofluorescein diacetate ($DCFH_2$-DA, Sigma-Aldrich®, USA) was incubated with the cells, which upon oxidation by the intracellular ROS was converted to a fluorescent product 2',7'-dichlorofluorescein (DCF). For that, 3×10^4 M2-like macrophages per well were seeded and allowed to attach overnight. Afterwards, 200 µg/mL of R848-loaded LNPs and a similar concentration of free R848 (2 µg/mL) in 100 µL of complete cell culturing medium were incubated with the cells for 30 min, at 37°C. Then, the wells were washed once with PBS (pH 7.4), and 100 µL of fresh cell culturing medium was added for 48 h, at 37°C. Finally, 100 µL of $DCFH_2$-DA (10 µM) in HBSS–HEPES buffer was incubated with the cells for 1h, at 37°C. Cells treated with cell culturing medium were used as control. Next, the fluorescence of the DCF (λ_{ex} = 498 nm and λ_{em} = 522 nm) was measured with a Varioskan Flash plate reader (Thermo Fisher Scientific Inc., USA).

2.11. Expression of cell surface markers on macrophages after *in vitro* repolarization of M2-like macrophages

The differentiation of M0 macrophages into M2-like macrophages was done in 48-plates after seeding 2.5×10^5 macrophages per well, in 500 µL of RPMI supplemented with 20 ng/mL of IL-4, during 48 h at 37°C. Then, 200 µg/mL of R848-loaded LNPs and a similar concentration of free R848 (ca. 2 µg/mL) were added to each well, in 300 µL of complete medium during 30 min at 37°C, and further replaced by 300 µL of fresh complete medium for 48 h at 37°C. The macrophages were then detached using 300 µL of PBS–EDTA (5 mM EDTA, for 15 min on ice), and the cell suspensions were centrifuged at 500*g* during 5 min. The samples were further incubated with 100 µL of TruStain FcX™ anti-mouse CD16/32 antibody (BioLegend, USA) in cold PBS for 10 min at 4°C, and then stained with anti-mouse Alexa Fluor 488–CD86 and APC–CD206 (BioLegend, USA) in cold PBS during 20 min at 4 °C. After washing twice with PBS (pH 7.4), the samples were analyzed by flow cytometry, using a LSR II flow

cytometer (BD Biosciences, USA) and FACS Diva software. The data were analyzed by FlowJo V10 software (Tree Star, Ashland, OR, USA) after collecting at least 20000 events.

2.12. Quantification of TNF-α levels

The amount of TNF-α secreted by the macrophages after differentiation and repolarization was quantified in the cell culture supernatant using an ELISA kit for TNF-α detection (ab46105, abcam®, USA), following the manufacturers' protocols.

2.13. *In vivo* evaluation of the biosafety of R848@LNPs

Healthy female Balb/c mice (6-8 week-old) were injected intraperitoneally with 200 µL of R848@LNPs-P-FAM or R848@LNPs-P-F-mUNO (250 µg) in 5.4% glucose, or 5.4% glucose as control, and circulated for 48 h (n = 3). Then, mice were anesthetized, and 500 µL of blood was collected by retro-orbital bleeding into lithium heparin tubes (BD Vacutainer 368494), centrifuged at 1800*g* for 15 min at 4°C, and 400 µL of the supernatant (plasma) was collected. Finally, the samples were analyzed for concentration of Creatinine in the Tartu University Hospital, using a Cobas 6000 IT-MW (Roche Diagnostics Gmbh) machine and reagent for creatinine CREP2 (cat 03263991).

2.14. *In vivo* tumor model

The 4T1 tumors were induced according to protocols approved by the Estonian Ministry of Agriculture, Committee of Animal Experimentation (permit #48). Female 8-12 week-old Balb/c mice (in-house bred) were inoculated orthotopically by injecting 1×10^6 4T1 cells dispersed in 50 µL of PBS in the 5th mammary fat pad. The tumor volume was calculated using the formula $(W^2 \times L)/2$, where W is the tumor width and L is the tumor length, and these dimensions were measured using a digital caliper (Mitutoyo).

2.15. *In vivo* homing study and *ex-vivo* biodistribution analysis

To evaluate the tumor homing of R848-loaded LNPs-P-FAM and LNPs-P-F-mUNO, 4T1 tumor-bearing mice were used 6 days after inoculation, when the tumors reached a volume of ca. 50 mm^3. Then, 250 µg of LNPs dispersed in 200 µL of 5.4% glucose were administered intraperitoneally. Three hours later, mice were sacrificed by intraperitoneal (i.p.) administration of 500 µL of 2.5% Avertin and cervical dislocation, the tumors and organs were excised, rinsed with PBS and placed in 4% PFA at 4°C, overnight. The tissues were then rinsed with PBS and left in PBS for 1 h at RT, to wash off any remaining PFA. Then, tissues were placed in 15% sucrose (in PBS) overnight, and later in 30% sucrose overnight. The tissues were frozen in Optimal Cutting Temperature (OCT, from Leica Biosystems, USA) blocks, from which 20 µm-thick sections were cut using a Leica cryotome, transferred onto glass slides (Super Frost glass, Thermofisher, USA) and stored at −20°C. For immunostaining, the tissue sections were thawed and left 2 h to dry at RT, in the dark. The immunostaining protocol used was the same as described elsewhere,(Scodeller et al., 2017) using rat anti-mouse CD206 (dilution 1:150) and rabbit anti-FAM (dilution 1:100) as the primary antibodies, and goat anti-rat Alexa Fluor 546 (dilution 1:200) and goat anti-rabbit Alexa Fluor 647 (dilution 1:200) as the secondary antibodies. The sections were counterstained with DAPI, mounted, sealed with nail polish and imaged with a Zeiss LSM-710 confocal microscope (Germany). The total FAM signal and colocalization (Pearson's coefficient) between the FAM channel and CD206 channel were performed using ImageJ, and the average values were obtained from at least 4 different images, obtained from 3 different tumors.

2.16. *In vivo therapeutic study*

On day 6 post-tumor inoculation, tumor volumes were measured using a digital caliper, and mice were sorted into 5 groups (n = 6) in order to have groups with tumor volume average of 46–48 mm^3. Then, mice were treated every other day with Vinblastine alone (1 mg/kg, in 500 µL of PBS, i.p.) or a combination of Vinblastine and 0.125 mg/kg of R848 (as free or nano-

formulated R848, in 200 µL of 5.4% glucose, i.p.). After day 12 post-tumor inoculation, Vinblastine was discontinued and the R848 administrations were continued every other day until day 16 post-tumor inoculation. Mouse weights and tumor volumes were measured at least every other day. On day 18 post-tumor inoculation all mice were sacrificed, and their tumors and organs were weighed. The tumors and organs from 3 mice from each group were used for immunological profile studies.

2.17. *Ex-vivo immunological profile of tumor and lymph node cells*

Single cell suspensions from tumor tissues were obtained after pre-incubation with 200 U/mL of Hyaluronidase (From Bovine Testes Sigma-Aldrich®, USA) for 2 h. Then, both lymph nodes and tumor tissues were gently disrupted of the tissue samples using a cell strainer (40 or 70 µm mesh, respectively) with a syringe plunger. Samples were suspended with FBS (containing 5% DMSO), and then cryopreserved at −80°C, until the day of analysis. After quickly thawing, the samples were incubated with ACK lysis buffer to get rid of the red blood cells, and washed once with PBS. Then, cells were incubated with TruStain FcX™ anti-mouse CD16/32 antibody (BioLegend, USA) in cold PBS for 10 min at RT, followed by the stainings with antibody mixtures for 20 min, at 4°C. Finally, samples were washed twice with PBS and analyzed by flow cytometry, using a BD Accuri 6 plus (BD Biosciences, USA), and the FlowJo V10 software was used for data analysis, after collecting 500000 events. Antibodies from BD Biosciences or BioLegend were used to stain cell surface markers for macrophages (PE-F4/80, and Alexa Fluor 488-CD86), T cells (Alexa Fluor 488-CD3ε, and APC-CD8), and DCs (FITC-CD11c and APC-CD86).

2.18. *Immunological profiling of tumor tissues*

Immunofluorescence analysis was used to perform the immunological profiling of tumor tissues after therapeutic study. Treated tissues were cryoprotected as previously described, frozen using OCT, and 10 µm-thick sections were cut using a Leica microtome, and further stored at −20°C. After 24 h, tissues were thawed and left at RT for at least 30 min. The immunostaining protocol used was the same as described elsewhere (Scodeller et al., 2017). To visualize M2 macrophage population, rat anti-mouse CD206 antibody (dilution 1:150) was used as primary antibody and Alexa 647 goat anti-rat (dilution 1:250, Invitrogen, cat A21247) as secondary antibody. For iNOS evaluation, rabbit anti-mouse iNOS (dilution 1:100, LSBio, cat LS-C352602-100) was used as primary antibody and Alexa 647 goat anti-rabbit (dilution 1:200) as secondary antibody. For IFN-γ measurement, rat anti-mouse primary antibody was used and Alexa 647 Goat anti-rat (dilution 1:200, Invitrogen, cat A21247) as secondary antibody. For CD8 evaluation, rat anti-mouse primary antibody was used and Alexa 647 goat anti-rat (dilution 1:200, Invitrogen, cat A21247) as secondary antibody. Tissue slides were counterstained with DAPI, mounted, sealed and imaged using Zeiss confocal microscope with 10 × objective. Mean pixel count was calculated using 8 representative images from three different tumors per group, with ImageJ program.

2.19. Statistical analysis

The measured values are expressed by mean ± standard deviation (s.d.) of at least three independent experiments. Statistical analysis was performed using the GraphPad Prism (GraphPad Software Inc., CA, USA). The probability was set as $*p < 0.05$, $**p < 0.01$ and $***p < 0.001$. Generally, one-way analysis of variance (ANOVA) with the Bonferroni's post-hoc-test was used to estimate the significant differences, with exception of the tumor weight data, where the Newman-Keuls Multiple Comparison Test was used. Additionally, two-way ANOVA was used for the statistical analysis of the tumor volume curves.

3. **Results and discussion**

3.1. **Preparation and characterization of the LNPs**

Firstly, the empty LNPs and R848@LNPs were prepared *via* solvent exchange, using the dialysis method described elsewhere (**Fig. 1A**) [50]. During this process, the carboxylated lignin polymer dissolved in THF, with or without R848, self-assembled into colloidal NPs as the THF was gradually replaced by MilliQ-water. Acting as a non-solvent, the water reduces lignin's degrees of freedom and causes the segregation of hydrophobic regions to compartments within the forming NPs, which also allowed the incorporation of R848 inside this compartment [50]. Afterwards, the –COOH groups on empty or R848-loaded LNPs were covalently bound to the $–NH_2$ groups of the NH_2-PEG-Maleimide (2K), using EDC/NHS coupling chemistry, rendering LNPs-PEG-Mal or R848@LNPs-PEG-Mal, respectively (**Fig. 1B**). The free cysteine groups on both FAM and F-mUNO reacted with the maleimide groups on empty or R848-loaded LNPs-PEG-Mal to yield LNPs-P-FAM or R848@LNPs-P-FAM and LNPs-P-F-mUNO or R848@LNPs-P-F-mUNO, respectively. All these formulations were further characterized for their average particle size, PDI, and ζ-potential by DLS, as shown in **Fig. 1C**. The empty LNPs presented an average size of 189 ± 8 nm, while the size of R848@LNPs slightly increased to 229 ± 36 nm after R848 loading. Moreover, the average size of the LNPs slightly increased after the PEGylation reaction, where the LNPs-PEG-Mal showed 273 ± 17 nm and the R848@LNPs-PEG-Mal 302 ± 42 nm. However, no significant changes in the average sizes of both empty and R848-loaded LNPs were observed after reaction with FAM or F-mUNO, and the maximum size obtained was for the LNPs-P-F-mUNO, which was 315 ± 13 nm. Regarding the size distribution, all the prepared LNPs and R848@LNPs presented PDI values lower than 0.25, suggesting a moderate polydispersity of the LNPs. Additionally, the empty LNPs were also characterized by ATR–FTIR and fluorescence of the FAM fluorochrome after conjugation reactions (**Fig. S1**). The ATR–FTIR spectra showed that the functionalized LNPs exhibited a characteristic band near 1670 cm^{-1} ascribed to the C=O stretching vibrations of the amide bond (O=C–NH). Moreover, both LNPs-P-FAM and LNPs-P-F-mUNO showed a stronger fluorescence signal due to the presence of the FAM fluorochrome, compared to the LNPs-PEG-Mal that does not exhibit any fluorescence. Overall, all these results suggested the success of the conjugation reactions.

The loading degree of R848 into LNPs was quantified by HPLC (**Table 1**), after dissolving the LNPs in ethanol to release the drug. The mass ratio used for loading R848 inside LNPs (1:10 of R848:LNPs) was chosen after finding the optimal ratio to have a good loading degree without increasing the average size of the R848@LNPs. The loading degree of R848 in the LNPs, LNPs-P-FAM, and LNPs-P-F-mUNO was 1.76 ± 0.20%, 1.14 ± 0.18%, and 1.02 ± 1.4%, respectively (**Fig. 1D**). The morphology and size distribution of the empty and R848-loaded LNPs was also verified by TEM (**Fig. 1E**), and the all LNPs presented symmetric and spherical shape, because of the interaction between the water and lignin during the dialysis process [50]. Furthermore, the morphology and size distribution of the LNPs did not change after the LNP surface functionalization, as well as after R848 loading into the LNPs.

3.2. Stability of the R848@LNPs and *in vitro* dissolution profiles of R848

The specificity and extent of protein binding to the NP's surface in physiological environment is influenced by the composition, shape, size and surface chemistry of the particles, which consequently affect their biofate upon administration [53,54]. Therefore, we evaluated the stability of the bare and functionalized R848@LNPs by measuring the changes on the size and PDI of the NPs, during their incubation in cell culture medium, supplemented with 10% of FBS, at 37°C for 2 h (**Fig. 2A,B**). Overall, the results showed an increase of about 50 nm in the R848@LNP size during the first minutes of incubation, which kept constant over time. Despite of the electrostatic repulsion between the negatively charged proteins and the NP's surface, this minor increase in the NP size might indicate some protein adsorption onto the NP's surface due to the FBS proteins [55]. However, the PDI of the NPs did not change significantly, suggesting that the aggregation of the NPs did not occur, probably due to the presence of FBS that can improve the colloidal stability of NPs [56].

Then, the R848 dissolution profiles of free R848 and R848@LNPs were evaluated in two different aqueous buffer solutions mimicking the tumor microenvironment/intracellular endosomes (pH 5.5) and the physiological pH (pH 7.4), during 24 h at 37°C (**Fig. 2C,D**). For the free R848, the dissolution was found to be below 40% at both pH values, mainly due to its relatively low water solubility. However, R848@LNPs showed a burst release at pH 5.5 and 7.4 of *ca.* 80 and 100% within 24 h, respectively. Our previous findings suggested that the release of the drugs can occur by a diffusion mechanism through the lignin structure [21]. Overall, these results indicated that LNPs can substantially improve the dissolution rate of the R848, and protect it inside the nanostructure as no degradation or precipitation of R848 was observed.

3.3. *In vitro* cell–LNP association studies and repolarization of M2-like macrophages

Next, we used primary mouse M2-like macrophages to perform the *in vitro* characterization of the formulation, *i.e.* cytocompatibility, cell–LNP binding and repolarization. For that, BMDMs were isolated and seeded in cell medium containing M-CSF for 6 days to obtain M0 macrophages ($F4/80^+$ $CD11b^+$), which were further differentiated into M1- or M2-like macrophages after incubation with LPS and IFN-γ or IL-4, respectively (**Fig. S2A**) [51]. These macrophages were characterized by measuring the expression of CD86 and CD206 cell surface markers, and their morphology was also observed (**Fig. S2B,C,E**). Here, M1-like macrophages showed higher expression of CD86 and a round shape, while M2-like macrophages presented higher expression of CD206 and a more elongated shape [57]. Additionally, the levels of TNF-α released by the macrophages was quantified in the cell culture supernatants by ELISA assay (**Fig. S2D**). As expected, M1-like macrophages released higher concentration of TNF-α compared to resting or M2-like macrophages [32,33]. Then, the cytocompatibility of empty and R848-loaded LNPs with mouse M2-like macrophages and 4T1 cells was evaluated after incubation for 24 h with different LNP concentrations, ranging from 25 to 200 µg/mL, and similar concentrations of free R848 (0.1–2 µg/mL) (**Fig. S3**). Both empty and R848-loaded LNPs were non-toxic towards the two cell lines for all the concentrations tested, also indicating that R848 did not interfere with the viability of macrophages or 4T1 cells.

The *in vitro* binding of empty LNPs to M2 macrophages was also evaluated both qualitatively and quantitatively, using confocal microscopy and flow cytometry, respectively. For this, 200 µg/mL of LNP-P-FAM and LNP-P-F-mUNO were incubated with M2 macrophages, and short time points (10, 30 and 60 min) were used to select the ideal incubation time for the repolarization study. In confocal microscopy (**Fig. 3A**), the LNP-P-F-mUNO showed a higher association with M2 macrophages than the control LNP-P-FAM for the three time points tested, which was confirmed after quantification of the co-localization of the FAM and CD206 channels (**Fig. 3B-D**). The LNP-P-F-mUNO showed higher co-localization with the CD206 on the M2 macrophages after 30 min of incubation. Binding of these formulations to M2 macrophages was also quantified by flow cytometry (**Fig. 3E**), where the LNP-P-F-mUNO showed *ca.* twice higher association with M2 macrophages after 30 min, compared to the LNP-P-FAM. Based on these results, we further studied the specificity of the targeting of mUNO-functionalized R848-loaded LNPs towards the $CD206^+$ M2 macrophages, and quantitatively evaluated the cellular association of R848@LNPs-P-F-mUNO (200 µg/mL) with M1-like macrophages, and M2-like macrophages, with and without previous blocking of the CD206 receptor, after 30 min of incubation (**Fig. S4**). The cellular association of R848@LNPs-P-F-mUNO with M2-like macrophages was about 1-fold higher compared to the M1-like macrophages. Furthermore, after blocking the CD206 receptor on M2 macrophages, the cellular association of R848@LNPs-P-F-mUNO decreased to similar values obtained for M1 macrophages. All these observations suggest that mUNO peptide improves the binding of LNPs to $CD206^+$ M2 macrophages, in particular after 30 min of incubation, and thus, we selected this time point for the subsequent studies.

For the repolarization study, 200 µg/mL of R848@LNP-P-FAM and R848@LNP-P-F-mUNO, containing about 2 µg/mL of R848, and similar concentration of free R848, were incubated with M2 macrophages for 30 min, which was then replaced by cell medium for an additional 48 h, at 37°C. Next, the expression of the cell surface markers (CD206 and CD86) was quantified using flow cytometry and normalized with the untreated control (**Fig. 3F**). Both R848@LNPs induced a higher expression of CD86 compared to the free R848, while decreasing the levels of CD206 cell surface marker, showing that the treatment with R848 can revert the macrophage phenotype from M2-like ($CD206^+$) into M1-like phenotype ($CD86^+$). In addition, increased production of ROS (*e.g.*, H_2O_2) after incubation with R848@LNP-P-F-mUNO was also observed, compared to the free R848, using the $DCFH_2$-DA assay (**Fig. 3G**). This is also an indication of the macrophage re-education towards the M1-like phenotype or anti-tumor effect, as these macrophages are known to produce more ROS, which can act as secondary messengers that regulate downstream pathways, and consequently, promote the expression of proinflammatory genes [58,59]. Furthermore, the concentration of TNF-α after treatment with free or nanoformulated R848 radically increased compared to the untreated control (**Fig. 3H**), and the incubation with R848@LNP-P-F-mUNO led to a significantly higher secretion of TNF-α than the free R848.

3.4. *In vivo* homing study and *ex-vivo* biodistribution analysis

Then, we used an orthotopic and highly aggressive 4T1 TNBC syngeneic model in immunocompetent Balb/c mice to investigate the biodistribution and homing of the LNPs. For this, both R848@LNPs-P-FAM and R848@LNPs-P-F-mUNO were injected i.p. in 4T1 tumor-bearing mice, and their ability to target the tumor was evaluated. After 3 h, mice were sacrificed and their organs were collected, cryoprotected and cryo-sectioned for biodistribution analysis by confocal microscopy (Fig. 4). The tumor sections showed that both R848@LNPs-P-FAM and R848@LNPs-P-F-mUNO showed similar patterns of accumulation in the TAMs at the tumor site (Fig. 4**A,B**), which was quantified by the co-localization of the FAM signal and CD206 signal (Fig. 4**C**). Here, the percentage of co-localization of both channels was about 50% and 60% for R848@LNPs-P-FAM and R848@LNPs-P-F-mUNO, respectively. However, when the intensity of the FAM signal was measured in the $CD206^+$ macrophages, the R848@LNPs-P-F-mUNO showed a significantly higher accumulation compared to the control R848@LNPs-P-FAM (Fig. 4**D**). This suggests that the mUNO peptide can effectively increase the interaction of empty LNPs or R848@LNPs with the M2-like macrophages in the TME. Additionally, the distribution of the R848@LNPs in the main organs was also evaluated (Fig. 4**A**). The accumulation of R848@LNPs in the lungs was very low, suggesting that almost no NP aggregates were formed. Furthermore, the accumulation of both nanosystems was low in the main organs responsible for the clearance of NPs (liver, spleen, and kidney), which can indicate that the NPs were either cleared out from these organs or at the M2 TAMs in the tumor after 3 h.

3.5. *In vivo* Therapeutic Study and *Ex-vivo* Immunological Profile of Tumor Tissues

Finally, we evaluated the ability of these nanosystems to potentiate the antitumor efficacy of the chemotherapeutic compound vinblastine (Vin), a vinca alkaloid and microtubule-destabilizing agent that affects cell growth and survival by disrupting the dynamic equilibrium of the microtubules, and blocks the cell cycle at the metaphase-anaphase transition in mitosis, leading to the cellular apoptosis [60]. For this study, we selected the water-soluble Vinblastine sulfate as the chemotherapeutic agent, due to its high potency towards different cell lines compared to other chemotherapeutic agents [61], and also because no effect of Vin on the viability of M2-like macrophages has been reported before, as these macrophages present none or minimal proliferation rates [31]. Vin has also been used in different therapeutic regimens in previously treated or advanced breast cancer patients [62,63]. Therefore, we aimed to combine the treatment with R848 to enhance the conventional chemotherapy (Vin), and therefore, potentiate the antitumor response.

Based on these, we decided to administer Vin at a dose of 1 mg/kg as monotherapy or combined with free R848 or R848@LNPs at *ca.* 0.125 mg/kg, using an orthotopic 4T1 TNBC model in immunocompetent Balb/c mice. On day 6 post-tumor inoculation, mice were randomized in 5 groups with average tumor volume of about 47 mm^3, and the following treatments were administered i.p.: (1) PBS and 5.4% of Glucose (Control); (2) Vin and 5.4% of Glucose (Vinblastine); (3) Vin and free R848 (Vin + R848); (4) Vin and R848@LNPs-P-FAM (Vin + R848@LNPs-P-FAM); and (5) Vin and R848@LNPs-P-F-mUNO (Vin + R848@LNPs-P-F-mUNO). The treatment schedule is schematized in Fig. 5**A**, where the free R848 or R848@LNPs was co-administered with the Vin every other day. The Vin treatment was interrupted when the dose-limiting toxicity was reached and the mice receiving Vin started losing weight (**Fig. S5**). Then, the treatment with free and nanoformulated R848 was continued until the endpoint, which was defined at day 18 post-tumor inoculation, in order to study the immunological profile of the cells in the tumors and lymph nodes. Additionally, the biosafety of R848@LNPs was assessed by measuring the levels of creatinine in the plasma of healthy mice, for the evaluation of kidney toxicity (**Fig. S6**). After 48 h of circulation time, both R848@LNPs-P-FAM and R848@LNPs-P-F-mUNO did not show kidney toxicity.

The Vin treatment showed some antitumor activity, as the tumor volume decreased compared to the PBS group (Fig. 5**A**). However, only R848@LNPs-P-F-mUNO was able to provide a statistically significant improvement of the Vin treatment, as evidenced by the tumor volume kinetics (Fig. 5**B**) and the tumor weight (Fig. 5**C**) at the end of the treatment. The non-targeted R848@LNPs-P-FAM showed a trend of improvement over the free R848 (Fig. 5**C**), which is in line with the results observed in the homing study, where both targeted and non-targeted R848@LNPs showed accumulation in $CD206^+$ TAMs. However, the

R848@LNPs showed an increased accumulation in the CD206$^+$ TAMs when targeted with the mUNO peptide, which led to an increased concentration of R848 in M2-like TAMs. Overall, these findings suggest that mUNO targeting of R848-loaded in a nanoplatform to M2-like macrophages at the TME can improve the antitumor efficacy compared to the free R848, by altering its pharmacokinetics and biodistribution upon administration.

Immune cells are known to have a critical role in the regulation of tumor growth, and therefore, we compared the immunological profile of the cells extracted from the tumors in the groups receiving free or nanoformulated R848, using flow cytometry (**Fig. 5D-F**), following the gating approach as shown in **Fig. S7**, as well as using immunofluorescence-based staining (representative images are shown in **Fig. S8**). Firstly, we assessed the modifications in the macrophage population in the tumor tissues, which are primarily defined by the presence of the F4/80 marker, and the M1 macrophage subsets were identified by the expression of CD86 markers [32,33]. Both non-targeted and mUNO-targeted R848@LNPs showed higher levels of F4/80$^+$CD86$^+$ macrophages, compared to the free R848 (**Fig. 5D**), suggesting that the delivery of R848 with LNPs can trigger in situ reprogramming of M2 TAMs into M1-like phenotype at the tumor tissue, compared to the free R848. This repolarization into M1-skewed macrophages can then initiate an anti-tumor response characterized by the release of pro-inflammatory signals (*e.g.*, TNF-α, IL-6, and IL-12) and production of ROS [32–34]. Additionally, endogenous inducible nitric oxide synthase (iNOS) has been associated with increased tumor aggressiveness, reduction of chemotherapeutic treatment efficacy, and poor survival rates in TNBC, and therefore, its inhibition seemed to decrease TNBC aggressiveness [64–66]. According to the immunofluorescence staining for iNOS in the tumor tissue, the treatment with mUNO-targeted R848@LNPs showed a decrease in the iNOS levels compared to the other two groups, especially compared with the non-targeted R848@LNPs (**Fig. 5G**). Additionally, the amount of CD206$^+$ cells in the tumor was higher for the treatment with the R848@LNPs-P-FAM compared to the R848@LNPs-P-FmUNO (**Fig. 5H**). Furthermore, the group receiving the R848@LNPs-P-FmUNO presented slightly higher amount of CD206$^+$ cells compared to the free R848. A similar effect was also observed by Galstyan *et al.* [67], which can be ascribed to the fact that the nanoscale treatment might not reach the necrotic areas of the tumor, which can contain M2 polarized macrophages, due to the extensive tissue necrosis and lack of vasculature in treated tumors. Therefore, the R848@LNPs-P-F-mUNO showed a slightly higher amount of CD206 positive cells compared to the group receiving R848.

The presence of M2 macrophages in the TME is also associated with the poor infiltration of cytotoxic T cells (CTLs) in the tumor, which is frequently associated with higher risk of relapse and a poor outcome in breast cancer patients [26,68]. However, TAMs depletion was shown to reestablish the T cell migration and infiltration into tumors [69]. Here, we used CD3 and CD8 as markers to evaluate the presence of CTLs (CD8$^+$ T cells) in the tumor tissues (**Fig. 5E**). The percentage of CD3$^+$CD8$^+$ T cells in the tumor was significantly higher for the group receiving the R848@LNPs-P-F-mUNO compared with the other two groups. The CD8 staining by immunofluorescence also confirmed the increase of the CD8$^+$ cells in the tumor after treatment with R848@LNPs-P-F-mUNO (**Fig. 5I**). This can be due to the indirect effect of the more efficient re-education of M2-macrophages accomplished by mUNO-targeted R848@LNPs. The reduction of the immunosuppressive microenvironment in the tumor can indirectly trigger the action of CD8$^+$ T cells, and directly activate T cell cytotoxicity caused by the release of ARG1, which ultimately leads to the T cell activation [70,71]. Thus, the tumor infiltration of CTLs can boost immune responses against the tumor, which is characterized by the secretion of IFN-γ [72]. The levels of IFN-γ quantified by immunofluorescence increased proportionally to the percentage of CD8$^+$ T cells in the TME, in which the treatment with R848@LNPs-P-F-mUNO resulted in a superior level of IFN-γ at the tumor tissue (**Fig. 5J**). The infiltration of tumor tissues by antigen-presenting cells (APCs), like dendritic cells (DCs), is also one of the main prognostic factors in cancer treatment because it can provide a second stimulatory signal to trigger the anti-tumor T cell response [70]. Therefore, we next evaluated the DCs' population in the tumor tissues, primarily characterized by the CD11c expression, and in particular the percentage of activated CD86$^+$ DCs (**Fig. 5F**). The delivery of R848 by LNPs led to a general increase in the percentage of CD86 positive DCs in the tumor compared with the free R848. In addition, we also characterized the cell population in the lymph nodes (**Fig. S9A–D**), in which a significantly higher percentage of M1-like macrophages (F4/80$^+$CD86$^+$) and CD11c$^+$CD80$^+$ DCs was observed after treatment with the mUNO-targeted R848@LNPs.

4. Conclusion

In this study, we successfully developed an effective lignin-based nanosystem to target a potent TLR7/8 agonist (R848) to the TME, in order to revert the tumor supportive (M2-like) macrophages into an anti-tumor (M1-like) phenotype, for enhanced chemotherapy. The use of mUNO to target the R848@LNPs to M2 macrophages showed an improved efficiency of the R848 in different ways, such as by modifying the biodistribution of the R848 and enhancing its accumulation and efficacy in shifting the immunological profile of the cells in the TME, not possible to achieve by systemic administration of free R848. Loading R848 into NPs can also decrease the systemic side effects associated with the repeated administration of TLR agonists in the free form, which is a limitation for their translation into the clinic [73,74]. Moreover, a reduction in the tumor volumes was achieved at lower equivalent doses of R848 compared with other studies [46,75]. Therefore, the co-administration of R848@LNPs is a promising candidate for chemotherapeutic applications in very aggressive tumors, such as the TNBC.

5. Statement of significance

Comment [AU1]: CE: Check placement of Hea `Statement of significance'.

Lignin-based nanoparticles (LNPs) were successfully developed to target a potent TLR7/8 agonist (R848) of the tumor microenvironment (TME). This was achieved by targeting the mannose receptor (CD206) on the tumor supportive (M2-like) macrophages with the “mUNO” peptide, to reprogram them into an anti-tumor (M1-like) phenotype for enhanced chemotherapy. LNPs modified the biodistribution of the R848, and enhanced its accumulation and efficacy in shifting the immunological profile of the cells in the TME, which was not achieved by systemic administration of free R848. Moreover, a reduction in the tumor volumes was observed at lower equivalent doses of R848 compared with other studies. Therefore, the co-administration of R848@LNPs is a promising chemotherapeutic application in aggressive tumors, such as the triple-negative breast cancer.

Uncited References:

Comment [AU2]: This section comprises references that occur in the reference list but not the body of the text. Please position each referer in the text or, alternatively, delete it.

[47, 48, 49, 52]

mmc1.docx

Declaration of Competing Interests

None

Acknowledgements

P. Figueiredo acknowledges the Finnish Cultural Foundation for a research grant (decision no. 00190246), and the financial support from the Orion Research Foundation and the NordForsk for the Nordic University Hub project #85352 (Nordic POP, Patient Oriented Products). P. Scodeller acknowledges a personal research grant from the Estonian Research Council (PUT PSG38). M. Tiboni acknowledges the Italian Ministry of Education, University and Research for the “Bando Leonardo da Vinci – Azione 2” travel grant (ID no. 159146). M.-A. Shahbazi acknowledges financial support from the Academy of Finland (grant no. 317316). T. Teesalu was supported by the European Regional Development Fund (Project No. 2014-2020.4.01.15-0012), by European Research Council grant GLIOGUIDE from European Regional Development Fund, and Estonian Research Council (grants PRG230 and EAG79). H. A. Santos acknowledges financial support from the Sigrid Jusélius Foundation, the HiLIFE Research Funds, the Academy of Finland (decision no. 317042) and the European Research Council Proof-of-Concept Grant (decision no. 825020). The authors thank the Flow Cytometry Unit of the Institute of Biotechnology and the Electron Microscopy Unit, University of Helsinki, for providing the necessary laboratory facilities and assistance.

References

<bib id="bib1" type="Periodical"><number>[1]</number> F. Fontana, P. Figueiredo, T. Bauleth-Ramos, A. Correia, H.A. Santos, Immunostimulation and Immunosuppression: Nanotechnology on the Brink, Small Methods. 2 (2018) 1700347.</bib>

<bib id="bib2" type="Periodical"><number>[2]</number> T. Bauleth-Ramos, M.-A. Shahbazi, D. Liu, F. Fontana, A. Correia, P. Figueiredo, H. Zhang, J.P. Martins, J.T. Hirvonen, P. Granja, B. Sarmento, H.A. Santos, Nutlin-3a and Cytokine Co-loaded Spermine-Modified Acetalated Dextran Nanoparticles for Cancer Chemo-Immunotherapy, Adv. Funct. Mater. 27 (2017) 1703303.</bib>

<bib id="bib3" type="Periodical"><number>[3]</number> F. Fontana, M.-A. Shahbazi, D. Liu, H. Zhang, E. Mäkilä, J. Salonen, J.T. Hirvonen, H.A. Santos, Multistaged Nanovaccines Based on Porous Silicon@Acetalated Dextran@Cancer Cell Membrane for Cancer Immunotherapy, Adv. Mater. 29 (2017) 1603239.</bib>

<bib id="bib4" type="Periodical"><number>[4]</number> F. Fontana, M. Fusciello, C. Groeneveldt, C. Capasso, J. Chiaro, S. Feola, Z. Liu, E.M. Mä, J.J. Salonen, J.T. Hirvonen, V. Cerullo, H.A. Santos, Biohybrid Vaccines for Improved Treatment of Aggressive Melanoma with Checkpoint Inhibitor, ACS Nano. 13 (2019) 6477--6490.</bib>

<bib id="bib5" type="Periodical"><number>[5]</number> M. Fusciello, F. Fontana, S. Tähtinen, C. Capasso, S. Feola, B. Martins, J. Chiaro, K. Peltonen, L. Ylösmäki, E. Ylösmäki, F. Hamdan, O.K. Karl, J. Ndika, H. Alenius, A. Urtti, J.T. Hirvonen, H.A. Santos, V. Cerullo, Artificially cloaked viral nanovaccine for cancer immunotherapy, Nat. Commun. 10 (2019) 5747.</bib>

<bib id="bib6" type="Periodical"><number>[6]</number> A. Wicki, D. Witzigmann, V. Balasubramanian, J. Huwyler, Nanomedicine in cancer therapy: Challenges, opportunities, and clinical applications, J. Control. Release. 200 (2015) 138--157.</bib>

<bib id="bib7" type="Periodical"><number>[7]</number> J. Shi, P.W. Kantoff, R. Wooster, O.C. Farokhzad, Cancer nanomedicine: Progress, challenges and opportunities, Nat. Rev. Cancer. 17 (2017) 20--37.</bib>

<bib id="bib8" type="Book"><number>[8]</number> P. Figueiredo, T. Bauleth-Ramos, J. Hirvonen, B. Sarmento, H.A. Santos, The Emerging Role of Multifunctional Theranostic Materials in Cancer Nanomedicine, in: Handb. Nanomater. Cancer Theranostics, Elsevier, 2018: pp. 1--31.</bib>

<bib id="bib9" type="Periodical"><number>[9]</number> A. Rahikkala, S.A.P. Pereira, P. Figueiredo, M.L.C. Passos, A.R.T.S. Araújo, M.L.M.F.S. Saraiva, H.A. Santos, Mesoporous Silica Nanoparticles for Targeted and Stimuli-Responsive Delivery of Chemotherapeutics: A Review, Adv. Biosyst. 2 (2018) 1800020.</bib>

<bib id="bib10" type="Periodical"><number>[10]</number> W. Li, Z. Liu, F. Fontana, Y. Ding, D. Liu, J.T. Hirvonen, H.A. Santos, Tailoring Porous Silicon for Biomedical Applications: From Drug Delivery to Cancer Immunotherapy, Adv. Mater. 30 (2018).</bib>

<bib id="bib11" type="Periodical"><number>[11]</number> T.M. Allen, P.R. Cullis, Liposomal drug delivery systems: From concept to clinical applications, Adv. Drug Deliv. Rev. 65 (2013) 36--48.</bib>

<bib id="bib12" type="Periodical"><number>[12]</number> R. Cheng, L. Liu, Y. Xiang, Y. Lu, L. Deng, H. Zhang, H.A. Santos, W. Cui, Advanced liposome-loaded scaffolds for therapeutic and tissue engineering applications, Biomaterials. 232 (2020).</bib>

<bib id="bib13" type="Periodical"><number>[13]</number> E. Wonder, L. Simón-Gracia, P. Scodeller, R.N. Majzoub, V.R. Kotamraju, K.K. Ewert, T. Teesalu, C.R. Safinya, Competition of charge-mediated and specific binding by peptide-tagged cationic liposome--DNA nanoparticles in vitro and in vivo, Biomaterials. 166 (2018) 52--63.</bib>

<bib id="bib14" type="Periodical"><number>[14]</number> V. Balasubramanian, B. Herranz-Blanco, P. V. Almeida, J. Hirvonen, H.A. Santos, Multifaceted polymersome platforms: Spanning from self-assembly to drug delivery and protocells, Prog. Polym. Sci. 60 (2016) 51--85.</bib>

<bib id="bib15" type="Periodical"><number>[15]</number> P. Figueiredo, V. Balasubramanian, M.A. Shahbazi, A. Correia, D. Wu, C.G. Palivan, J.T. Hirvonen, H.A. Santos, Angiopep2-functionalized polymersomes for targeted doxorubicin delivery to glioblastoma cells, Int. J. Pharm. 511 (2016) 794--803.</bib>

<bib id="bib16" type="Periodical"><number>[16]</number> B. Herranz-Blanco, M.-A. Shahbazi, A.R. Correia, V. Balasubramanian, T. Kohout, J. Hirvonen, H.A. Santos, pH-Switch Nanoprecipitation of Polymeric Nanoparticles for Multimodal Cancer Targeting and Intracellular Triggered Delivery of Doxorubicin, Adv. Healthc. Mater. 5 (2016) 1904--1916.</bib>

<bib id="bib17" type="Periodical"><number>[17]</number> S. Wannasarit, S. Wang, P. Figueiredo, C. Trujillo, F. Eburnea, L. Simón-Gracia, A. Correia, Y. Ding, T. Teesalu, D. Liu, R. Wiwattanapatapee, H.A. Santos, W. Li, A Virus-Mimicking pH-Responsive Acetalated Dextran-Based Membrane-Active Polymeric Nanoparticle for Intracellular Delivery of Antitumor Therapeutics, Adv. Funct. Mater. 29 (2019) 1905352.</bib>

<bib id="bib18" type="Periodical"><number>[18]</number> L. Simón-Gracia, H. Hunt, P. Scodeller, J. Gaitzsch, V.R. Kotamraju, K.N. Sugahara, O. Tammik, E. Ruoslahti, G. Battaglia, T. Teesalu, iRGD peptide conjugation potentiates intraperitoneal tumor delivery of paclitaxel with polymersomes, Biomaterials. 104 (2016) 247--257.</bib>

<bib id="bib19" type="Periodical"><number>[19]</number> P. Figueiredo, K. Lintinen, J.T. Hirvonen, M.A. Kostiainen, H.A. Santos, Properties and chemical modifications of lignin: Towards lignin-based nanomaterials for biomedical applications, Prog. Mater. Sci. 93 (2018) 233--269.</bib>

<bib id="bib20" type="Periodical"><number>[20]</number> S. Imlimthan, A. Correia, P. Figueiredo, K. Lintinen, V. Balasubramanian, A.J. Airaksinen, M.A. Kostiainen, H.A. Santos, M. Sarparanta, Systematic in vitro biocompatibility studies of multimodal cellulose nanocrystal and lignin nanoparticles, J. Biomed. Mater. Res. Part A. 108 (2020) 770--783.</bib>

<bib id="bib21" type="Periodical"><number>[21]</number> P. Figueiredo, K. Lintinen, A. Kiriazis, V. Hynninen, Z. Liu, T. Bauleth-Ramos, A. Rahikkala, A. Correia, T. Kohout, B. Sarmento, J. Yli-Kauhaluoma, J. Hirvonen, O. Ikkala, M.A. Kostiainen, H.A. Santos, In vitro evaluation of biodegradable lignin-based nanoparticles for drug delivery and enhanced antiproliferation effect in cancer cells, Biomaterials. 121 (2017) 97--108.</bib>

<bib id="bib22" type="Periodical"><number>[22]</number> M.H. Sipponen, H. Lange, M. Ago, C. Crestini, Understanding Lignin Aggregation Processes. A Case Study: Budesonide Entrapment and Stimuli Controlled Release from Lignin Nanoparticles, ACS Sustain. Chem. Eng. 6 (2018) 9342--9351.</bib>

<bib id="bib23" type="Periodical"><number>[23]</number> K. Lintinen, Y. Xiao, R. Bangalore Ashok, T. Leskinen, E. Sakarinen, M. Sipponen, F. Muhammad, P. Oinas, M. Österberg, M. Kostiainen, Closed cycle production of

concentrated and dry redispersible colloidal lignin particles with a three solvent polarity exchange method, Green Chem. 20 (2018) 843--850.</bib>

<bib id="bib24" type="Periodical"><number>[24]</number> P. Figueiredo, C. Ferro, M. Kemell, Z. Liu, A. Kiriazis, K. Lintinen, H.F. Florindo, J. Yli-Kauhaluoma, J. Hirvonen, M.A. Kostiainen, H.A. Santos, Functionalization of carboxylated lignin nanoparticles for targeted and pH-responsive delivery of anticancer drugs, Nanomedicine. 12 (2017) 2581--2596.</bib>

<bib id="bib25" type="Periodical"><number>[25]</number> P. Figueiredo, M.H. Sipponen, K. Lintinen, A. Correia, A. Kiriazis, J. Yli-Kauhaluoma, M. Österberg, A. George, J. Hirvonen, M.A. Kostiainen, H.A. Santos, Preparation and Characterization of Dentin Phosphophoryn-Derived Peptide-Functionalized Lignin Nanoparticles for Enhanced Cellular Uptake, Small. 15 (2019) 1901427.</bib>

<bib id="bib26" type="Periodical"><number>[26]</number> G. Bianchini, J.M. Balko, I.A. Mayer, M.E. Sanders, L. Gianni, Triple-negative breast cancer: challenges and opportunities of a heterogeneous disease, Nat. Rev. Clin. Oncol. 13 (2016) 674--690.</bib>

<bib id="bib27" type="Periodical"><number>[27]</number> W.D. Foulkes, I.E. Smith, J.S. Reis-Filho, Triple-negative breast cancer, N. Engl. J. Med. 363 (2010) 1938--1948.</bib>

<bib id="bib28" type="Periodical"><number>[28]</number> N. Volodko, T. Gutor, O. Petronchak, R. Huley, M. Dúcka, J. Šmarda, L. Borsig, P. Beneš, L. Knopfová, Low infiltration of tumor-associated macrophages in high c-Myb-expressing breast tumors, Sci. Rep. 9 (2019) 11634.</bib>

<bib id="bib29" type="Periodical"><number>[29]</number> Z.Y. Yuan, R.Z. Luo, R.J. Peng, S. Sen Wang, C. Xue, High infiltration of tumor-associated macrophages in triple-negative breast cancer is associated with a higher risk of distant metastasis, Onco. Targets. Ther. 7 (2014) 1475--1480.</bib>

<bib id="bib30" type="Periodical"><number>[30]</number> M.J. Campbell, N.Y. Tonlaar, E.R. Garwood, D. Huo, D.H. Moore, A.I. Khramtsov, A. Au, F. Baehner, Y. Chen, D.O. Malaka, A. Lin, O.O. Adeyanju, S. Li, C. Gong, M. McGrath, O.I. Olopade, L.J. Esserman, Proliferating macrophages associated with high grade, hormone receptor negative breast cancer and poor clinical outcome, Breast Cancer Res. Treat. 128 (2011) 703--711.</bib>

<bib id="bib31" type="Periodical"><number>[31]</number> A. Mantovani, F. Marchesi, A. Malesci, L. Laghi, P. Allavena, Tumour-associated macrophages as treatment targets in oncology, Nat. Rev. Clin. Oncol. 14 (2017) 399--416.</bib>

<bib id="bib32" type="Periodical"><number>[32]</number> P. Allavena, A. Sica, G. Solinas, C. Porta, A. Mantovani, The inflammatory micro-environment in tumor progression: The role of tumor-associated macrophages, Crit. Rev. Oncol. Hematol. 66 (2008) 1--9.</bib>

<bib id="bib33" type="Periodical"><number>[33]</number> Y. Chen, Y. Song, W. Du, L. Gong, H. Chang, Z. Zou, Tumor-associated macrophages: An accomplice in solid tumor progression, J. Biomed. Sci. 26 (2019) 49.</bib>

<bib id="bib34" type="Periodical"><number>[34]</number> A.R. Poh, M. Ernst, Targeting macrophages in cancer: From bench to bedside, Front. Oncol. 8 (2018).</bib>

<bib id="bib35" type="Periodical"><number>[35]</number> L. Malorni, P.B. Shetty, C. De Angelis, S. Hilsenbeck, M.F. Rimawi, R. Elledge, C.K. Osborne, S. De Placido, G. Arpino, Clinical and biologic features of triple-negative

breast cancers in a large cohort of patients with long-term follow-up, Breast Cancer Res. Treat. 136 (2012) 795--804.</bib>

<bib id="bib36" type="Periodical"><number>[36]</number> C.H. Ries, M.A. Cannarile, S. Hoves, J. Benz, K. Wartha, V. Runza, F. Rey-Giraud, L.P. Pradel, F. Feuerhake, I. Klaman, T. Jones, U. Jucknischke, S. Scheiblich, K. Kaluza, I.H. Gorr, A. Walz, K. Abiraj, P.A. Cassier, A. Sica, C. Gomez-Roca, K.E. deVisser, A. Italiano, C. LeTourneau, J.P. Delord, H. Levitsky, J.Y. Blay, D. Rüttinger, Targeting tumor-associated macrophages with anti-CSF-1R antibody reveals a strategy for cancer therapy, Cancer Cell. 25 (2014) 846--859.</bib>

<bib id="bib37" type="Periodical"><number>[37]</number> S.M. Pyonteck, L. Akkari, A.J. Schuhmacher, R.L. Bowman, L. Sevenich, D.F. Quail, O.C. Olson, M.L. Quick, J.T. Huse, V. Teijeiro, M. Setty, C.S. Leslie, Y. Oei, A. Pedraza, J. Zhang, C.W. Brennan, J.C. Sutton, E.C. Holland, D. Daniel, J.A. Joyce, CSF-1R inhibition alters macrophage polarization and blocks glioma progression, Nat. Med. 19 (2013) 1264--1272.</bib>

<bib id="bib38" type="Periodical"><number>[38]</number> B.Z. Qian, J. Li, H. Zhang, T. Kitamura, J. Zhang, L.R. Campion, E.A. Kaiser, L.A. Snyder, J.W. Pollard, CCL2 recruits inflammatory monocytes to facilitate breast-tumour metastasis, Nature. 475 (2011) 222--225.</bib>

<bib id="bib39" type="Periodical"><number>[39]</number> X. Li, R. Liu, X. Su, Y. Pan, X. Han, C. Shao, Y. Shi, Harnessing tumor-associated macrophages as aids for cancer immunotherapy, Mol. Cancer. 18 (2019) 177.</bib>

<bib id="bib40" type="Periodical"><number>[40]</number> W. He, N. Kapate, C. Wyatt Shields, S. Mitragotri, Drug delivery to macrophages: A review of targeting drugs and drug carriers to macrophages for inflammatory diseases, Adv. Drug Deliv. Rev. (2019).</bib>

<bib id="bib41" type="Periodical"><number>[41]</number> L. Yang, Y. Zhang, Tumor-associated macrophages, potential targets for cancer treatment, Biomark. Res. 5 (2017) 25.</bib>

<bib id="bib42" type="Periodical"><number>[42]</number> M.-A. Shahbazi, M. Sedighi, T. Bauleth-Ramos, K. Kant, A. Correia, N. Poursina, B. Sarmento, J. Hirvonen, H.A. Santos, Targeted Reinforcement of Macrophage Reprogramming Toward M2 Polarization by IL-4-Loaded Hyaluronic Acid Particles, ACS Omega. 3 (2018) 18444--18455.</bib>

<bib id="bib43" type="Periodical"><number>[43]</number> X. Zheng, K. Turkowski, J. Mora, B. Brüne, W. Seeger, A. Weigert, R. Savai, Redirecting tumor-associated macrophages to become tumoricidal effectors as a novel strategy for cancer therapy, Oncotarget. 8 (2017) 48436--48452.</bib>

<bib id="bib44" type="Periodical"><number>[44]</number> M. Ovais, M. Guo, C. Chen, Tailoring Nanomaterials for Targeting Tumor-Associated Macrophages, Adv. Mater. 31 (2019) 1808303.</bib>

<bib id="bib45" type="Book"><number>[45]</number> P. Figueiredo, F. Fontana, H.A. Santos, Nanomedicine Therapies, in: Handb. Vivo Chem. Mice, Wiley, 2020: pp. 373--400.</bib>

<bib id="bib46" type="Periodical"><number>[46]</number> C.B. Rodell, S.P. Arlauckas, M.F. Cuccarese, C.S. Garris, R. Li, M.S. Ahmed, R.H. Kohler, M.J. Pittet, R. Weissleder, TLR7/8-agonist-loaded nanoparticles promote the polarization of tumour-associated macrophages to enhance cancer immunotherapy, Nat. Biomed. Eng. 2 (2018) 578--588.</bib>

<bib id="bib47" type="Periodical"><number>[47]</number> P. Scodeller, L. Simón-Gracia, S. Kopanchuk, A. Tobi, K. Kilk, P. Säälik, K. Kurm, M.L. Squadrito, V.R. Kotamraju, A. Rinken, M. De Palma, E. Ruoslahti, T. Teesalu, Precision Targeting of Tumor Macrophages with a CD206 Binding Peptide, Sci. Rep. 7 (2017).</bib>

<bib id="bib48" type="Periodical"><number>[48]</number> E.K. Asciutto, S. Kopanchuk, A. Lepland, L. Simón-Gracia, C. Aleman, T. Teesalu, P. Scodeller, Phage-Display-Derived Peptide Binds to Human CD206 and Modeling Reveals a New Binding Site on the Receptor, J. Phys. Chem. B. 123 (2019) 1973--1982.</bib>

<bib id="bib49" type="Periodical"><number>[49]</number> A. Lepland, E.K. Asciutto, A. Malfanti, L. Simón-Gracia, V. Sidorenko, M.J. Vicent, T. Teesalu, P. Scodeller, Targeting pro-tumoral macrophages in early primary and metastatic breast tumors with CD206-binding mUNO peptide, Mol. Pharm. (2020) acs.molpharmaceut.0c00226.</bib>

<bib id="bib50" type="Periodical"><number>[50]</number> M. Lievonen, J.J. Valle-Delgado, M.L. Mattinen, E.L. Hult, K. Lintinen, M.A. Kostiainen, A. Paananen, G.R. Szilvay, H. Setälä, M. Österberg, A simple process for lignin nanoparticle preparation, Green Chem. 18 (2016) 1416--1422.</bib>

<bib id="bib51" type="Periodical"><number>[51]</number> W. Ying, P.S. Cheruku, F.W. Bazer, S.H. Safe, B. Zhou, Investigation of Macrophage Polarization Using Bone Marrow Derived Macrophages, J. Vis. Exp. (2013) 50323.</bib>

<bib id="bib52" type="Periodical"><number>[52]</number> P. Scodeller, L. Simón-Gracia, S. Kopanchuk, A. Tobi, K. Kilk, P. Säälik, K. Kurm, M.L. Squadrito, V.R. Kotamraju, A. Rinken, M. De Palma, E. Ruoslahti, T. Teesalu, Precision Targeting of Tumor Macrophages with a CD206 Binding Peptide, Sci. Rep. 7 (2017) 14655.</bib>

<bib id="bib53" type="Periodical"><number>[53]</number> P. Aggarwal, J.B. Hall, C.B. McLeland, M.A. Dobrovolskaia, S.E. McNeil, Nanoparticle interaction with plasma proteins as it relates to particle biodistribution, biocompatibility and therapeutic efficacy, Adv. Drug Deliv. Rev. 61 (2009) 428--437.</bib>

<bib id="bib54" type="Periodical"><number>[54]</number> M. Hadjidemetriou, K. Kostarelos, Nanomedicine: Evolution of the nanoparticle corona, Nat. Nanotechnol. 12 (2017) 288--290.</bib>

<bib id="bib55" type="Periodical"><number>[55]</number> S.R. Saptarshi, A. Duschl, A.L. Lopata, Interaction of nanoparticles with proteins: Relation to bio-reactivity of the nanoparticle, J. Nanobiotechnology. 11 (2013) 26.</bib>

<bib id="bib56" type="Periodical"><number>[56]</number> T.L. Moore, L. Rodriguez-Lorenzo, V. Hirsch, S. Balog, D. Urban, C. Jud, B. Rothen-Rutishauser, M. Lattuada, A. Petri-Fink, Nanoparticle colloidal stability in cell culture media and impact on cellular interactions, Chem. Soc. Rev. 44 (2015) 6287--6305.</bib>

<bib id="bib57" type="Periodical"><number>[57]</number> R. Sridharan, A.R. Cameron, D.J. Kelly, C.J. Kearney, F.J. O'Brien, Biomaterial based modulation of macrophage polarization: A review and suggested design principles, Mater. Today. 18 (2015) 313--325.</bib>

<bib id="bib58" type="Periodical"><number>[58]</number> H.Y. Tan, N. Wang, S. Li, M. Hong, X. Wang, Y. Feng, The Reactive Oxygen Species in Macrophage Polarization: Reflecting Its Dual Role in Progression and Treatment of Human Diseases, Oxid. Med. Cell. Longev. (2016) 2795090.</bib>

<bib id="bib59" type="Periodical"><number>[59]</number> B. Griess, S. Mir, K. Datta, M. Teoh-Fitzgerald, Scavenging reactive oxygen species selectively inhibits M2 macrophage polarization and their pro-tumorigenic function in part, via Stat3 suppression, Free Radic. Biol. Med. 147 (2020) 48--60.</bib>

<bib id="bib60" type="Periodical"><number>[60]</number> F. Pellegrini, D.R. Budman, Review: Tubulin function, action of antitubulin drugs, and new drug development, Cancer Invest. 23 (2005) 264--273.</bib>

<bib id="bib61" type="Periodical"><number>[61]</number> A. Roy, M.J. Ernsting, E. Undzys, S.-D. Li, A highly tumor-targeted nanoparticle of podophyllotoxin penetrated tumor core and regressed multidrug resistant tumors, Biomaterials. 52 (2015) 335--346.</bib>

<bib id="bib62" type="Periodical"><number>[62]</number> I. Ospovat, N. Siegelmann-Danieli, T. Grenader, A. Hubert, T. Hamburger, T. Peretz, Mitomycin C and vinblastine: an active regimen in previously treated breast cancer patients., Tumori. 95 (n.d.) 683--6.</bib>

<bib id="bib63" type="Periodical"><number>[63]</number> A. Urruticoechea, C.D. Archer, L.A. Assersohn, R.K. Gregory, M. Verrill, R. Mendes, G. Walsh, I.E. Smith, S.R.D. Johnston, Mitomycin C, vinblastine and cisplatin (MVP): An active and well-tolerated salvage regimen for advanced breast cancer, Br. J. Cancer. 92 (2005) 475--479.</bib>

<bib id="bib64" type="Periodical"><number>[64]</number> P. Garrido, A. Shalaby, E.M. Walsh, N. Keane, M. Webber, M.M. Keane, F.J. Sullivan, M.J. Kerin, G. Callagy, A.E. Ryan, S.A. Glynn, Impact of inducible nitric oxide synthase (iNOS) expression on triple negative breast cancer outcome and activation of EGFR and ERK signaling pathways, Oncotarget. 8 (2017) 80568--80588.</bib>

<bib id="bib65" type="Periodical"><number>[65]</number> Z. Jin, W. Wang, N. Jiang, L. Zhang, Y. Li, X. Xu, S. Cai, L. Wei, X. Liu, G. Chen, Y. Zhou, C. Liu, Z. Li, F. Jin, B. Chen, Clinical implications of iNOS levels in triple-negative breast cancer responding to neoadjuvant chemotherapy, PLoS One. 10 (2015).</bib>

<bib id="bib66" type="Periodical"><number>[66]</number> S. Granados-Principal, Y. Liu, M.L. Guevara, E. Blanco, D.S. Choi, W. Qian, T. Patel, A.A. Rodriguez, J. Cusimano, H.L. Weiss, H. Zhao, M.D. Landis, B. Dave, S.S. Gross, J.C. Chang, Inhibition of iNOS as a novel effective targeted therapy against triple-negative breast cancer, Breast Cancer Res. 17 (2015) 25.</bib>

<bib id="bib67" type="Periodical"><number>[67]</number> A. Galstyan, J.L. Markman, E.S. Shatalova, A. Chiechi, A.J. Korman, R. Patil, D. Klymyshyn, W.G. Tourtellotte, L.L. Israel, O. Braubach, V.A. Ljubimov, L.A. Mashouf, A. Ramesh, Z.B. Grodzinski, M.L. Penichet, K.L. Black, E. Holler, T. Sun, H. Ding, A. V. Ljubimov, J.Y. Ljubimova, Blood--brain barrier permeable nano immunoconjugates induce local immune responses for glioma therapy, Nat. Commun. 10 (2019).</bib>

<bib id="bib68" type="Periodical"><number>[68]</number> S. Aaltomaa, P. Lipponen, M. Eskelinen, V.M. Kosma, S. Marin, E. Alhava, K. Syrjänen, Lymphocyte infiltrates as a prognostic variable in female breast cancer, Eur. J. Cancer. 28 (1992) 859--864.</bib>

<bib id="bib69" type="Periodical"><number>[69]</number> E. Peranzoni, J. Lemoine, L. Vimeux, V. Feuillet, S. Barrin, C. Kantari-Mimoun, N. Bercovici, M. Guérin, J. Biton, H. Ouakrim, F. Régnier, A. Lupo, M. Alifano, D. Damotte, E. Donnadieu, Macrophages impede CD8 T cells from reaching tumor cells and limit the efficacy of anti--PD-1 treatment, Proc. Natl. Acad. Sci. U. S. A. 115 (2018) E4041--E4050.</bib>

<bib id="bib70" type="Periodical"><number>[70]</number> L. Cassetta, J.W. Pollard, Targeting macrophages: therapeutic approaches in cancer, Nat. Rev. Drug Discov. 17 (2018) 887--904.</bib>

<bib id="bib71" type="Periodical"><number>[71]</number> R. Noy, J.W. Pollard, Tumor-Associated Macrophages: From Mechanisms to Therapy, Immunity. 41 (2014) 49--61.</bib>

<bib id="bib72" type="Periodical"><number>[72]</number> S.Y. Gun, S.W.L. Lee, J.L. Sieow, S.C. Wong, Targeting immune cells for cancer therapy, Redox Biol. 25 (2019).</bib>

<bib id="bib73" type="Periodical"><number>[73]</number> P.J. Pockros, D. Guyader, H. Patton, M.J. Tong, T. Wright, J.G. McHutchison, T.C. Meng, Oral resiquimod in chronic HCV infection: Safety and efficacy in 2 placebo-controlled, double-blind phase IIa studies, J. Hepatol. 47 (2007) 174--182.</bib>

<bib id="bib74" type="Periodical"><number>[74]</number> A. Thomas, C. Laxton, J. Rodman, N. Myangar, N. Horscroft, T. Parkinson, Investigating toll-like receptor agonists for potential to treat hepatitis C virus infection, Antimicrob. Agents Chemother. 51 (2007) 2969--2978.</bib>

<bib id="bib75" type="Periodical"><number>[75]</number> C.B. Rodell, M.S. Ahmed, C.S. Garris, M.J. Pittet, R. Weissleder, Development of Adamantane-Conjugated TLR7/8 Agonists for Supramolecular Delivery and Cancer Immunotherapy, Theranostics. 9 (2019) 8426--8436.</bib>

Fig. 1. Schematic representation of the solvent exchange process to prepare the empty or R848-loaded LNPs (**A**) and further conjugation reactions (**B**). Characterization of bare and R848-loaded LNPs, before and after functionalization by measuring (**C**) the average size, PDI, and ζ-potential of the LNPs; (**D**) quantification of the loading degree of R848 and (**E**) TEM images of the empty LNPs (scale bars = 200 nm). Error bars represent the mean ± s.d. ($n \geq 3$).

Fig. 2. Stability of LNPs after 2 h incubation in RPMI supplemented with 10% of FBS, at 37°C: effect on the (**A**) size and (**B**) PDI. Dissolution profiles of pure R848, R848@LNPs-P-FAM and R848@LNPs-P-F-mUNO in (**C**) HBSS–MES (pH 5.5) and (**D**) HBSS–HEPES (pH 7.4) at 150 rpm and 37°C for 24 h. Errors bars represent mean ± s.d. ($n = 3$).

Fig. 3. *In vitro* cellular interaction studies of functionalized LNPs with M2-like macrophages. (**A**) Confocal fluorescence microscopy images after incubation with 200 μg/mL of LNPs-P-FAM and LNPs-P-F-mUNO for 10, 30 and 60 min at 37°C. DAPI (blue), anti-FAM (green), and anti-CD206 (red) were used to stain the nucleus, the LNPs, and the CD206 receptor, respectively. The merged panels show the association of the LNPs with the CD206 receptors (scale bars are 50 μm). Quantification of the co-localization of FAM and CD206 channels (Pearson's coefficient) after incubation with both LNPs for (**B**) 10 min, (**C**) 30 min, and (**D**) 60 min, using ImageJ ($n \geq 4$). (**E**) Quantitative cellular association by flow cytometry, after incubation of 200 μg/mL of LNPs-P-FAM and LNPs-P-F-mUNO, for 10, 30 and 60 min at 37°C. At least 20000 events were collected for each measurement ($n = 3$). *In vitro* repolarization of M2-like macrophages after incubation with 200 μg/mL of R848@LNPs-P-FAM, R848@LNPs-P-F-mUNO and free R848 (*ca.* 2 μg/mL) for 30 min, followed by incubation with cell medium for 48 h at 37°C. (**F**) Fold-change in the mean fluorescence intensity (MFI) values (relative to the untreated control, and normalized by the empty LNPs values), in the

expression CD206 and CD86 on macrophages, using flow cytometry; and (**G**) fold-increase in the production of ROS, compared to the untreated control and normalized by the empty LNPs values, was determined with a fluorescent $DCFH_2$-DA assay ($n = 3$). (**H**) Quantification of the TNF-α concentration in the cell culture supernatants using an ELISA assay ($n = 3$), after the repolarization study in which 200 µg/mL of R848@LNPs-P-FAM, R848@LNPs-P-F-mUNO and free R848 (*ca*. 2 µg/mL) for 30 min, followed by incubation with cell medium for 48 h at 37°C. The results were analyzed with one-way ANOVA followed by Bonferroni post-test, and statistical significance was set at probabilities of $*p < 0.05$, $**p < 0.01$, and $***p < 0.001$.

Fig. 4. Biodistribution of R848@LNPs-P-FAM and R848@LNPs-P-F-mUNO (250 µg), injected i.p. into 4T1 tumor-bearing mice ($n = 3$), and circulated for 3 h: (**A**) representative confocal fluorescence microscopy images of the *ex-vivo* biodistribution of the R848@LNPs, compared to the non-injected control (stained with secondary antibodies). DAPI (blue), anti-FAM (green), and anti-CD206 (red) were used to stain the nucleus, the LNPs, and CD206, respectively. (**B**) Enlarged images of the R848@LNPs distribution at the tumor. Scale bars are 100 µm. (**C**) Quantification of co-localization (Pearson's coefficient) between FAM and CD206 channels, and (**D**) total FAM signal per $CD206^+$ cells, using ImageJ ($n \geq 4$). The results were analyzed with one-way ANOVA followed by Bonferroni post-test, and statistical significance was set at the probability of $***p < 0.001$.

Fig. 5. *In vivo* therapeutic study using a 4T1 tumor-bearing mice ($n = 6$). (**A**) Therapeutic scheme, in which the red arrows represent the Vin injections (1 mg/kg, in 500 µL of PBS, i.p.), and the blue arrows indicate free or nanoformulated R848 administrations (0.125 mg/kg of R848, in 200 µL of 5.4% glucose, i.p.). (**B**) Tumor volumes measured with a digital caliper during the treatment ($n = 6$), and the results were analyzed with two-way ANOVA. (**C**) Tumor weights measured at the end of the treatment (day 18 post-tumor inoculation, $n = 6$), and the results were analyzed with one-way ANOVA followed by Newman-Keuls post-test. Analysis of the immunological profile of tumor cell population after treatment ($n = 3$), using flow cytometry: (**D**) macrophages; (**E**) T cells, and (**F**) dendritic cells. At least 500000 events were collected for each measurement. Immunofluorescence-based staining of tumor tissue after treatment ($n = 3$) for (**G**) iNOS; (**H**) $CD206^+$ cells (M2 macrophages); (**I**) $CD8^+$ cells (T cells), and (**J**) INF-γ. Quantification of mean pixel count using ImageJ ($n \geq 8$). The results (**D**–**J**) were analyzed with one-way ANOVA followed by Bonferroni post-test. Statistical significance was set at probabilities of $*p < 0.05$, $**p < 0.01$, and $***p < 0.001$.

Table 1. HPLC conditions used in this study for quantification of the loaded R848.

Mobile Phase (v/v)	Solution A: 0.1% Trifluoroacetic acid (pH 2.0)
Solution B: Acetonitrile	
Ratio A:B (Gradient)	0–3 min: 100:0
3–5 min: 5:95	

5–8 min: 100:0	
Column	Kinetex® C_{18}, 75 mm × 4.6 mm, 2.6 µm (Phenomenex, USA)
Flow Rate (mL/min)	1.0
Detection (UV, nm)	254 ± 5
Injection Volume (µL)	25
Temperature (°C)	25